Chirality-induced Spin Selectivity in Functionalized Carbon Nanotube Networks: The Role of Spin-orbit Coupling

Seyedamin Firouzeh,[a] Sara Illescas-López,[b] Md. Anik Hossain,[a] Juan Manuel Cuerva,[b] Luis Álvarez de Cienfuegos,[b,c,*] Sandipan Pramanik[a,*]

[a] Department of Electrical and Computer Engineering, University of Alberta, Alberta T6G 1H9, Canada

[b] Universidad de Granada, Departamento de Química Orgánica, Unidad de Excelencia Química Aplicada a Biomedicina y Medioambiente, C. U. Fuentenueva, Avda. Severo Ochoa s/n, E-18071 Granada, Spain

[c] Instituto de Investigación Biosanitaria ibs. Avda. De Madrid, 15, E-18016 Granada, Spain

*Corresponding Authors: lac@ugr.es, spramani@ualberta.ca

Abstract

Spin-orbit coupling of a chiral medium is generally assumed to be a necessary ingredient for the observation of the chirality-induced spin selectivity (CISS) effect. However, some recent studies have suggested that CISS may manifest even when the chiral medium has zero spin-orbit coupling. In such systems CISS may arise due to an orbital polarization effect, which generates an electromagnetochiral anisotropy in two-terminal conductance. Here, we examine these concepts using a chiral functionalized carbon nanotube network as the chiral medium. A *transverse* measurement geometry is used which nullifies any electromagnetochiral contribution, but still exhibits the tell-tale signs of the CISS effect. This suggests that CISS may not be explained solely by electromagnetochiral effects. The role of nanotube spin-orbit coupling on the observed *pure* CISS signal is studied by systematically varying nanotube diameter. We find that the *magnitude* of the CISS signal scales proportionately with the spin-orbit coupling strength of the nanotubes. We also find that nanotube diameter dictates the supramolecular chirality of the medium, which in turn determines the *sign* of the CISS signal.

I. INTRODUCTION.

The phenomenon of chirality-induced spin selectivity or CISS has recently attracted significant global attention, due to its potential implications in various fields such as spintronics, optoelectronics, enantioseparation, and spin-selective electrochemical and biological processes.[1,2] The key observation underpinning the CISS effect is that the chiral structures, for which the mirror images are non-superimposable, exhibit a preference to transmit a particular orientation of spin (up or down).[1,2] Such phenomenon can potentially be exploited to realize efficient non-magnetic, molecular scale spin filters, which are not only critical for miniaturization of spintronic devices, but also because they may enable novel device designs to control spins for various quantum technologies.[1,3]

Many organic molecules such as DNA, amino acids, polypeptides, helicenes etc. are chiral, and hence they are commonly used in a vast majority of studies on CISS.[4–7] Transmission of spin unpolarized electrons (typically injected from a non-magnetic Au contact) through the chiral molecules imparts spin polarization, which is detected by a magnetic contact such as Ni. However, these molecules behave as insulators in terms of their bulk electronic conductivity, which limits their device applications. CISS experiments on *single* or *few* molecules typically involve magnetoconductance measurements using an atomic force microscopic (AFM) tip.[5,7,8] Due to the uncertainty in forming good tip-molecule contact, such measurements show significant fluctuations, thereby necessitating computation of statistical average over many scans taken under nominally identical conditions. Experiments done in a *solid-state device* configuration, where transport occurs through a large ensemble of molecules, typically show weaker signals, presumably due to inhomogeneous spin polarization contributions from different non-equivalent current paths.[7–9] Recently, CISS has also been reported in chiral crystals,[10,11] and hybrid perovskites.[12,13]

Another emerging system for studying CISS in the *solid-state device* context is artificial *higher order nanostructures* in which conductive materials of superior electronic and spintronic properties (such as various two-dimensional (2D) van der Waals crystals) are integrated with chiral molecules to create chiral nanostructures with complex forms and hierarchy. Ref.[14] reported a structure in which chiral molecules are intercalated between the 2D atomic layers of TaS_2 and TiS_2. A similar structure has been reported in ref.[15], where chiral molecules are intercalated between the 2D atomic layers of MoS_2. In both of these cases, electronic transport occurs in the out-of-plane direction, and hence the observed CISS effect arises purely due to the transport of carriers through the chiral molecules in the interlayer regions. While the 2D layers offer structural stability and robustness to the devices, their planar electronic properties remain largely untapped. Thus, conceptually, these are very similar to the earlier experiments discussed above.

In principle, CISS can manifest in magnetotransport experiments performed on *conductive* inorganic nanostructures with non-zero spin-orbit coupling, subjected to a chiral electrostatic potential induced by attached chiral molecules. In such systems, charge transport should primarily occur via the conductive inorganic crystal, since the attached molecules are insulators beyond the tunneling regime of transport. The charge carriers, however, experience the chiral potential during transit, which, combined with spin-orbit coupling, is expected to polarize the spins via the CISS effect.

Carbon nanotubes (CNTs) are particularly interesting in this regard, because they behave as one-dimensional molecular conductors whose electronic properties are determined by delocalized molecular orbitals that are extended along their lengths. More importantly, they can be functionalized by a vast selection of chiral molecules as reported in the literature.[16,17] Such functionalizations are often non-covalent in nature, implying minimal deterioration of the intrinsic crystal structure of the CNTs. CNT functionalization using single stranded DNA was first reported in refs.[18,19] Possibility of observing CISS effect in such systems was investigated theoretically in refs.[20,21], and demonstrated experimentally in refs.[22–25] Such experiments typically probe *few* CNTs, and large signals can be observed at low temperatures.[22–24]

CNTs can be functionalized using chiral peptides as well.[26–29] The CISS effect in such systems has been reported in refs.[30–32] It has been found that the CISS effect survives structural heterogeneity of a planar random network, albeit at the cost of reduced signal strength compared to the "few tubes" configuration mentioned above. It has also been found that the global supramolecular chirality dictates the CISS signal, instead of the chirality of the molecular units or the chirality of the nanotubes.[31] CISS signal can be tuned in such systems by introducing small amounts of chiral "dopants", which can effectively invert the supramolecular chirality of the system.[31] Given the emergence of random CNT networks as a competitive material for solution-processed thin-film electronics, the above results open a way to introduce spintronic functionalities in such applications.[33,34]

Theoretical understanding of CISS continues to remain an open problem.[2] Three necessary ingredients for the observation of CISS have been identified, such as (a) spin-orbit coupling, (b) structural inversion asymmetry (introduced by medium chirality) and (c) time reversal asymmetry (typically introduced by magnetic field in magnetotransport experiments). Recently ref.[35] suggested that the spin-orbit coupling of the metal electrode is more important than that of the chiral media. In this model, one can ignore the spin-

orbit coupling of the chiral medium, and treat it as a polarizer of carrier orbital angular momentum. The spin-orbit coupling in the electrodes converts the orbital polarization to spin polarization, thereby resulting in CISS effect. This mechanism gives rise to an electromagnetochiral (EMCh) response, with resistance of the form $R(B,I) = R_0 - R^{\chi}B.I$, where R_0 is ordinary resistance, R^{χ} is the chirality dependent resistance, B is the magnetic field, and I represents current.[36] Recently, it has been suggested that such EMCh effect could give rise to the CISS effect by modulating the tunnel barrier between the contacts in CISS experiments.[37]

To examine these issues, we have recently studied the CISS effect in chiral functionalized planar CNT networks using a *transverse* configuration, in which the applied magnetic field is *perpendicular* to the current paths.[32] The tell-tale signs of the CISS effect have still been observed, indicating non-zero spin components transverse to the current direction.[32] It is important to note that in this *transverse* configuration the EMCh contribution is zero (since $B.I = 0$), and hence the observed response can be considered as a *pure* CISS signal, devoid of any other spurious chiral effects. The next question is *does the spin-orbit coupling of the CNTs contribute to this pure CISS signal*? Although graphene, the parent material of CNTs, has very weak spin-orbit coupling due to low atomic number of elemental carbon, CNTs, on the other hand show strong spin-orbit coupling due to orbital mixing induced by curvature.[38–40] For example, intrinsic spin-orbit effects in graphene is expected to appear at energy scales of ~1μeV, whereas in the case of SWCNTs, it is ~100μeV–1meV.[39,41,42] Curvature induced spin-orbit coupling in CNTs typically has the following form: $\Gamma \sim \gamma a \Delta_A^{SOC}/R$, where γ is a parameter which can range between 0.01–1, a is nearest neighbor carbon-carbon distance, Δ_A^{SOC} is the atomic spin-orbit interaction of carbon and R is the nanotube radius.[21] Thus, CNT radius is an experimental handle that allows tuning of the spin-orbit interaction and could affect the CISS signal. Double wall (DW) and multi wall (MW) tubes typically have larger diameters and therefore, they could be used for this investigation.

II. RESULTS AND DISCUSSIONS.

To test the above hypothesis, we studied planar CNT networks functionalized with Fmoc-diphenylalanine (or, Fmoc-FF) + glucono-δ-lactone (GdL). Molecular structures of these chiral moieties are shown in Figure S3 (Supplementary Information). We considered single wall (SW), double wall (DW) and multi wall (MW) tubes, with multi wall tubes having higher than two shells. A typical cross-sectional image of these tubes is schematically shown in Figure 1(a), with SW-, DW- and MWCNTs having *average* diameters of ~0.82 nm, ~0.9 nm, and ~9.5 nm respectively, as specified by the vendor. Diameters of SW- and DW-CNTs have been confirmed independently by us from the Raman radial breathing mode (RBM)

of the *raw* tubes, as discussed in the Supplementary Information Section (Figure S1). The diameter of MWCNTs can also be estimated from a Scanning Electron Microscopic (SEM) image as shown in Figure 1(b), although it's important to note that these tubes are attached with molecules, so they tend to exhibit larger diameters.

Synthesis of functionalized CNT networks has been reported before.[30–32] Briefly, a CNT suspension is created in a basic aqueous solution of Fmoc-FF via sonication. Next, GdL is added, which lowers the pH, resulting in the collapse of the peptide molecules and formation of a three-dimensional peptide hydrogel network, encapsulating the CNTs. The network formation takes place via π-π interaction and hydrogen bonding between the peptide molecules as well as between the peptide molecules and CNT sidewalls.[26] Since the FF side chain is chiral, its interaction with the CNTs is expected to induce chirality dependent effects in magnetotransport measurements. Additional experimental details are available in the Supplementary Information section.

For the fabrication of the device, a slice of the gel is placed between Ni-Au contact pairs fabricated on SiO_2/Si. The Ni contact is protected by a photoresist layer to prevent oxidation, which is only removed immediately before placing the gel. The Au and Ni contacts are made significantly large in dimension to minimize the contact resistance contributions in the two-terminal CISS measurements. Finally, the sample is annealed, which results in a xerogel structure contacted by Ni-Au. The device made in this procedure remains electrically stable for at least several weeks. An SEM image of the final device structure is shown in Figure 1(b).

Figure 1(c) shows the Raman spectra of the *functionalized* CNTs. The *G* band appears in all samples, typically at ~1580–1600 cm^{-1}, and is due to the longitudinal vibrations of the carbon atoms in the graphitic lattice. A weak shoulder peak is also observed in the *G* band, which is due to the tangential vibrations of the carbon atoms. Presence of a strong *G* peak in all cases indicates that the underlying graphitic lattice is mostly unaffected even after functionalization. All samples show a defect (*D*) peak around ~1350 cm^{-1}, which typically manifests after the sonication step (ref. "Experimental Details" in Supplementary Information) due to the broken ends of the tubes. Thus, MWCNTs naturally have a stronger *D* band, which is consistent with past studies.[43,44] The *G*' (or, 2*D*) band is observed around ~2680 cm^{-1}. In some cases small peaks are observed at ~2930 cm^{-1}, which is attributed to the *G*+*D* peak.[44] Low energy radial breathing modes (RBM) are absent in *functionalized* DW- and MWCNTs. This is due to the fact that the RBM frequency depends inversely on tube diameter (Supplementary Information) and the large diameter

of these tubes makes the detection of RBM difficult. Also, the attached molecules may cause suppression of radial vibration. However, RBM peaks are present in *functionalized* SWCNTs in the range of 260–280 cm^{-1}.

Figure 1(d) shows temperature-dependent resistance (R vs. T) of functionalized SW-, DW- and MWCNT samples in the range 10K–300K. In all cases we observe negative temperature coefficient of resistance *i.e.* the resistance decreases with increasing temperature ($dR/dT < 0$), which is consistent with earlier work on CNT networks.[45–49] Such behavior is generally explained by a "heterogeneous transport" model.[50] In a CNT network like ours, there exist potential barriers due to tube defects and inter-tube crossings, which will localize charge carriers in the nanotube segments. Carrier transport occurs via transport inside each nanotube segment coupled with phonon-assisted tunneling or hopping from one segment to another (schematically shown in Figure 1(a)). Narrower tubes (SW, DW) have larger band gaps compared to the MW tubes, resulting in a more semiconducting type behavior inside the tube segments. Thus, the overall resistance of the SW- and DW tubes are more sensitive to temperature compared to the MW tubes, which is observed in Figure 1(d). Multiple samples (~10) of each tube type have been tested, and each sample has been scanned multiple times. The error bars from these measurements are indicated in Figure 1(d), which shows that the $R(T)/R(300\ K)$ response is remarkably consistent. It is to be noted that in our case the nanotube walls are attached with chiral molecules, and hence the carriers in the nanotubes will experience a chiral potential as well as spin-orbit interaction of the nanotube.

For the magnetoresistance (MR) measurements we choose a *transverse* configuration, in which the magnetic field, and hence Ni magnetization is *perpendicular* to the sample plane and hence *perpendicular* to any in-plane current path (Figure 1(b)). Most studies in CISS employ a longitudinal configuration, in which the magnetic field is collinear with the current, and a spin component collinear to the current is detected.[1] However, signals from such geometry may have a contribution from the EMCh effect due to the non-zero $B.I$ term as discussed above. The transverse geometry chosen here tunes out any such contributions. Our earlier work has shown that even in this transverse configuration a clear CISS signal can be observed, which indicates the presence of a spin component transverse to the direction of the current.[32] Such transverse CISS signals can be viewed as a *pure* CISS signal, devoid of any artifacts arising from the EMCh effect.

MR effect in CNT networks, consisting of both SW- and MWCNTs, has been reported by multiple groups.[45–48,51–54] In all cases, negative MR is observed in a transverse geometry *i.e.* resistance R decreases

with increasing magnetic field (B) strength, at low temperatures and low magnetic fields. The negative MR is often attributed to quantum interference induced localization effects, and is *symmetric* relative to the magnetic field, i.e. R (+ B) = R (– B). In our experiments, the CNT network is functionalized with chiral molecules and they are contacted with one magnetic (Ni) and one non-magnetic (Au) electrode. As shown in Figures 2(a), (c), (e), we also observe a low temperature, low field negative MR for SW-, DW- and MWCNTs respectively. The key difference is that the MR is no longer symmetric relative to B, i.e. R (+ B) ≠ R (– B), and this *asymmetry* (or, the "tilting") of the MR curves is dependent on the chirality of the functionalized CNT network, as shown clearly in the *insets* of Figures 2(a), (c), (e). As shown in our earlier work, if achiral molecules are used, the MR response regains its symmetry.[30] According to the standard CISS picture, chiral medium polarizes electron spin, which experiences different transmission probabilities through the Ni electrode depending on its magnetization, resulting in an asymmetric $R(B)$ response.

To isolate the asymmetric component due to the CISS effect, we plot the asymmetric and symmetric components of the MR response in Figures 2(b), (d), (f), computed as $R^{Sym/Asym} = [R(B) \pm R(-B)]/2$. It is clear that the asymmetric component is chirality dependent. The *magnitudes* of the symmetric and the asymmetric components are computed as $\delta^{Sym} = R^{Sym}(0) - R^{Sym}(\pm 10kG)$ and $\delta^{Asym} = |R^{Asym}(+10kG) - R^{Asym}(-10kG)|$, and the normalized signal is computed as $\delta^{Asym}/\delta^{Sym} \times 100\%$.

Figure 3(a) shows the $\delta^{Asym}/\delta^{Sym}$ ratio for SW-, DW- and MWCNTs. Clearly the CISS-induced asymmetry of the MR signals decreases with increasing number of walls (or, *average* tube diameter). Multiple (~10) samples have been tested for each type of CNT, and each sample has been scanned multiple times. The corresponding error bars are shown in Figure 3(a). The above trend is always observed – i.e. MWCNT signals are always weaker than that of SWCNTs, while DWCNTs typically show an intermediate signal strength. In literature, the CISS signal is often computed as $\delta^{CISS} = [R(-10kG) - R(+10kG)]/min[R(\pm 10kG)] x\ 100\%$,[1] and $|\delta^{CISS}|$ is plotted in Figure 3(b). Clearly, $|\delta^{CISS}|$ for MWCNTs is weaker by an *order of magnitude* compared to that of SWCNTs and DWCNTs. The error bars in Figure 3(b) indicate that this observation is consistent from sample to sample.

MWCNTs consist of multiple coaxial graphene cylinders of different diameters. In most experiments, including ours, the MWCNTs are contacted by bulk metallic pads, which form electrical contact only with the outermost shell, and hence current is injected and extracted via the outermost graphene cylinder. This

is described schematically in Figure 1(a). Combined with the weak coupling between the shells, which prohibits inter-shell electron hopping at low temperatures, earlier experiments have reported that current flows primarily through the outermost shell.[55,56] Although the presence of defects in the CNT walls can cause some inter-shell hopping, the outermost shell is expected to be the primary conduction channel due to the above reason, which is also attached with chiral molecules and the carriers are subjected to the chiral potential. As discussed before, we consider the *mean* diameters of DW- and MWCNTs, which are estimated to be ~ 0.9 nm and ~ 9.5 nm respectively. Clearly, there exists an *order of magnitude* difference in the diameters between SW-/DWCNTs (~ 0.82 nm and ~ 0.9 nm respectively) and MWCNTs (~ 9.5 nm), which should result in an order of magnitude reduction of the spin-orbit coupling strength of MWCNTs compared to SW-/DWCNTs. This is expected to result in a concomitant *order of magnitude* reduction in the CISS signal for MWCNTs, which we indeed observe in Figure 3(b). Comparing $|\delta^{CISS}|$ of SWCNTs and DWCNTs, they differ by a factor of ~2.2, whereas their diameters differ by a factor of ~ 1.1, which are relatively close values and within the same *order of magnitud*e. Therefore, the systematic reduction of the CISS signal with nanotube radius, as observed in Figure 3(b), can be attributed to the gradual reduction of the CNT spin-orbit coupling with increasing radius.

Figure 3(c) shows the $\delta^{Asym}/\delta^{Sym}$ ratio for SW-, DW- and MWCNTs at different temperatures. A monotonic decreasing trend is observed, which has been reported before in CNT-based systems,[30–32] presumably due to increased spin relaxation in CNTs at higher temperatures.[57] At all temperatures SWCNT signal is the strongest, MWCNT is the weakest and DWCNT has an intermediate value. This is consistent from sample-to-sample, as indicated by the error bars. We also note that the CISS signal manifests in the 10K–30K range, which corresponds to an energy scale of 0.86 meV–2.58 meV. This matches with the ~1meV spin-orbit energy scale of CNTs discussed above.

In CNTs, bandgap depends inversely on diameter, and the larger-diameter multiwall tubes tend to be metallic. This explains why the MWCNT resistance is much smaller than SW/DW-CNT resistance values as seen in Figure 2. This metallic behavior of MWCNTs is also visible in Figure 1(d), where it shows much weaker temperature dependence compared to SW/DW-CNTs.

The trends reported above are based on normalized quantities such as $\delta^{Asym}/\delta^{Sym}$ and δ^{CISS}, and not on specific resistance values. Further, we have shown data from multiple samples (~10), and each sample has been tested multiple times. The error bars are indicated in our data. Our conclusions are based on the

overall statistical trend, and not on any specific device. Thus we believe that device-to-device variation has already been factored-in in our conclusions.

A curious feature of the MR responses is that the SWCNT samples exhibit *opposite* chirality dependent behavior compared to the DW and MW samples, as seen from Figures 2(b), (d), (f). To understand this, we investigate the circular dichroism (CD) response of the *diluted* CNT samples (Figure 4; also see Supplementary Information for HT spectra), which suggests that an inversion of the supramolecular chirality of the peptide fibers is taking place mediated by the type of nanotube. This effect is well-known in literature, as supramolecular interactions are non-covalent and can be affected by several internal and external stimuli such as chiral or achiral molecules, different additives, and changes in the pH of the media, solvent composition or by the application of heat, light or sonication.[58–60] Recently, it has been shown that supramolecular chirality can be inverted by the size of Au nanoparticles (NPs) through the interaction of the organic molecules with the different curvatures of the NPs.[61] Presumably, a similar effect is occurring here, as different CNT samples have a different radius and hence different curvature. Figure 4(a) shows the usual supramolecular arrangement of these type of peptides corresponding to a β-sheet and characterized by the presence of two peaks: one at ~270 nm (π - π^* transition of the fluorenyl groups) and the other more intense peak at ~220 nm (π - π^* transition of the amino acids).[62] The CD spectra of the Fmoc-FF (L) derivative (red color) showed negative values while the D derivative (blue color) showed positive values. Figure 4(b) shows the CD spectra of the peptide solutions (Fmoc-FF) at the same concentration but now interacting with a suspension of SWCNT (0.35%). In this case, the interaction with the SW tubes produced an inversion of the supramolecular chirality of the peptides, now showing positive values for the L derivative (red color) and negative values for the D derivative (blue color). Nevertheless, this inversion in the chirality was not observed for the other two samples containing DW- and MWCNT (Figures 4(c) and (d)). In these cases, the sign of the curves was the same as the initial Fmoc-FF peptide solutions of Figure 4(a). As such, the opposite CISS values of SWCNT samples with respect to DW- and MWCNTs (as observed in Figure 2) can be explained based on the opposite supramolecular chirality of the peptide-CNT samples.[8,31]

III. CONCLUSIONS.

To summarize, the physical origin of CISS is often debated, in particular the role of spin-orbit interaction of the chiral medium, and the effect of other EMCh effects on CISS. In this study, we nullified the EMCh effect using a transverse geometry, but still observed the characteristic CISS signals. The strength of this *pure* CISS signal scales proportionately with the spin-orbit strength of the medium. Thus, CISS cannot be

explained solely based on EMCh and spin-orbit coupling of the medium indeed plays a critical role. Spin-orbit coupling is generally considered to be a “double-edged sword" in spintronics, because on one hand it allows external electric field control of the spin orientations, but on the other hand, it can also cause spin dephasing. It appears that in CISS systems, spin signal actually increases with the spin-orbit coupling strength, which is different from conventional materials. The CISS signal is dictated by the supramolecular chirality of the medium, consistent with previous studies.

SUPPLEMENTARY INFORMATION

Supplementary Information includes I. Experimental details, II. CNT diameter estimation from Raman RBM data, III. HT spectra, IV. Molecular structures of Fmoc-FF and GdL.

ACKNOWLEDGMENTS

This study was supported by Projects P18-FR-3533 and A-FQM-340-UGR20 funded by FEDER/Junta de Andalucía-Consejería de Transformación Económica, Industria, Conocimiento y Universidades (Spain). S.P. acknowledges support from NFRFE-2019-01298 (New Frontiers in Research Fund – Exploration) and NSERC (Natural Sciences and Engineering Research Council) Canada, project RGPIN-2018-05127.

Notes.

The authors declare no competing financial interests.

REFERENCES

[1] C.D. Aiello, J.M. Abendroth, M. Abbas, A. Afanasev, S. Agarwal, A.S. Banerjee, D.N. Beratan, J.N. Belling, B. Berche, A. Botana, J.R. Caram, G.L. Celardo, G. Cuniberti, A. Garcia-Etxarri, A. Dianat, I. Diez-Perez, Y. Guo, R. Gutierrez, C. Herrmann, J. Hihath, S. Kale, P. Kurian, Y.-C. Lai, T. Liu, A. Lopez, E. Medina, V. Mujica, R. Naaman, M. Noormandipour, J.L. Palma, Y. Paltiel, W. Petuskey, J.C. Ribeiro-Silva, J.J. Saenz, E.J.G. Santos, M. Solyanik-Gorgone, V.J. Sorger, D.M. Stemer, J.M. Ugalde, A. Valdes-Curiel, S. Varela, D.H. Waldeck, M.R. Wasielewski, P.S. Weiss, H. Zacharias, and Q.H. Wang, “A Chirality-Based Quantum Leap,” ACS Nano **16**(4), 4989–5035 (2022).
[2] F. Evers, A. Aharony, N. Bar-Gill, O. Entin-Wohlman, P. Hedegård, O. Hod, P. Jelinek, G. Kamieniarz, M. Lemeshko, K. Michaeli, V. Mujica, R. Naaman, Y. Paltiel, S. Refaely-Abramson, O. Tal, J. Thijssen, M. Thoss, J.M. van Ruitenbeek, L. Venkataraman, D.H. Waldeck, B. Yan, and L. Kronik, “Theory of Chirality Induced Spin Selectivity: Progress and Challenges,” Adv. Mater. **34**(13), 2106629 (2022).
[3] K. Michaeli, V. Varade, R. Naaman, and D.H. Waldeck, “A new approach towards spintronics–spintronics with no magnets,” J. Phys. Condens. Matter **29**(10), 103002 (2017).

[4] B. Gohler, V. Hamelbeck, T.Z. Markus, M. Kettner, G.F. Hanne, Z. Vager, R. Naaman, and H. Zacharias, “Spin Selectivity in Electron Transmission Through Self-Assembled Monolayers of Double-Stranded DNA,” Science **331**(6019), 894–897 (2011).
[5] Z. Xie, T.Z. Markus, S.R. Cohen, Z. Vager, R. Gutierrez, and R. Naaman, “Spin Specific Electron Conduction through DNA Oligomers,” Nano Lett. **11**(11), 4652–4655 (2011).
[6] O.B. Dor, S. Yochelis, S.P. Mathew, R. Naaman, and Y. Paltiel, “A chiral-based magnetic memory device without a permanent magnet,” Nat. Commun. **4**(1), 1–6 (2013).
[7] V. Kiran, S.P. Mathew, S.R. Cohen, I.H. Delgado, J. Lacour, and R. Naaman, “Helicenes—A New Class of Organic Spin Filter,” Adv. Mater. **28**(10), 1957–1962 (2016).
[8] C. Kulkarni, A.K. Mondal, T.K. Das, G. Grinbom, F. Tassinari, M.F.J. Mabesoone, E.W. Meijer, and R. Naaman, “Highly Efficient and Tunable Filtering of Electrons’ Spin by Supramolecular Chirality of Nanofiber-Based Materials,” Adv. Mater. **32**(7), 1904965 (2020).
[9] S.P. Mathew, P.C. Mondal, H. Moshe, Y. Mastai, and R. Naaman, “Non-magnetic organic/inorganic spin injector at room temperature,” Appl. Phys. Lett. **105**(24), 242408 (2014).
[10] A. Inui, R. Aoki, Y. Nishiue, K. Shiota, Y. Kousaka, H. Shishido, D. Hirobe, M. Suda, J. Ohe, J. Kishine, H.M. Yamamoto, and Y. Togawa, “Chirality-Induced Spin-Polarized State of a Chiral Crystal CrNb3S6,” Phys. Rev. Lett. **124**(16), 166602 (2020).
[11] K. Shiota, A. Inui, Y. Hosaka, R. Amano, Y. Ōnuki, M. Hedo, T. Nakama, D. Hirobe, J. Ohe, J. Kishine, H.M. Yamamoto, H. Shishido, and Y. Togawa, “Chirality-Induced Spin Polarization over Macroscopic Distances in Chiral Disilicide Crystals,” Phys. Rev. Lett. **127**(12), 126602 (2021).
[12] H. Lu, J. Wang, C. Xiao, X. Pan, X. Chen, R. Brunecky, J.J. Berry, K. Zhu, M.C. Beard, and Z.V. Vardeny, “Spin-dependent charge transport through 2D chiral hybrid lead-iodide perovskites,” Sci. Adv. **5**(12), eaay0571 (2019).
[13] Y.-H. Kim, Y. Zhai, H. Lu, X. Pan, C. Xiao, E.A. Gaulding, S.P. Harvey, J.J. Berry, Z.V. Vardeny, J.M. Luther, and M.C. Beard, “Chiral-induced spin selectivity enables a room-temperature spin light-emitting diode,” Science **371**(6534), 1129–1133 (2021).
[14] Q. Qian, H. Ren, J. Zhou, Z. Wan, J. Zhou, X. Yan, J. Cai, P. Wang, B. Li, Z. Sofer, B. Li, X. Duan, X. Pan, Y. Huang, and X. Duan, “Chiral molecular intercalation superlattices,” Nature **606**(7916), 902–908 (2022).
[15] Z. Bian, K. Kato, T. Ogoshi, Z. Cui, B. Sa, Y. Tsutsui, S. Seki, and M. Suda, “Hybrid Chiral MoS2 Layers for Spin-Polarized Charge Transport and Spin-Dependent Electrocatalytic Applications,” Adv. Sci. **9**(17), 2201063 (2022).
[16] H. Kuzmany, A. Kukovecz, F. Simon, M. Holzweber, Ch. Kramberger, and T. Pichler, “Functionalization of carbon nanotubes,” Synth. Met. **141**(1), 113–122 (2004).
[17] A. Hirsch, and O. Vostrowsky, in *Funct. Mol. Nanostructures* --, edited by A.D. Schlüter (Springer, Berlin, Heidelberg, 2005), pp. 193–237.
[18] M. Zheng, A. Jagota, E.D. Semke, B.A. Diner, R.S. Mclean, S.R. Lustig, R.E. Richardson, and N.G. Tassi, “DNA-assisted dispersion and separation of carbon nanotubes,” Nat. Mater. **2**(5), 338–342 (2003).
[19] M. Zheng, A. Jagota, M.S. Strano, A.P. Santos, P. Barone, S.G. Chou, B.A. Diner, M.S. Dresselhaus, R.S. Mclean, G.B. Onoa, G.G. Samsonidze, E.D. Semke, M. Usrey, and D.J. Walls, “Structure-Based Carbon Nanotube Sorting by Sequence-Dependent DNA Assembly,” Science **302**(5650), 1545–1548 (2003).
[20] G.S. Diniz, A. Latgé, and S.E. Ulloa, “Helicoidal Fields and Spin Polarized Currents in Carbon Nanotube–DNA Hybrids,” Phys. Rev. Lett. **108**(12), 126601 (2012).
[21] Y. Perlitz, and K. Michaeli, “Helical liquid in carbon nanotubes wrapped with DNA molecules,” Phys. Rev. B **98**(19), 195405 (2018).
[22] K.M. Alam, and S. Pramanik, “Spin Filtering through Single-Wall Carbon Nanotubes Functionalized with Single-Stranded DNA,” Adv. Funct. Mater. **25**(21), 3210–3218 (2015).
[23] K.M. Alam, and S. Pramanik, “Spin filtering with poly-T wrapped single wall carbon nanotubes,” Nanoscale **9**(16), 5155–5163 (2017).
[24] Md.W. Rahman, K.M. Alam, and S. Pramanik, “Long Carbon Nanotubes Functionalized with DNA and Implications for Spintronics,” ACS Omega **3**(12), 17108–17115 (2018).
[25] Md.W. Rahman, S. Firouzeh, V. Mujica, and S. Pramanik, “Carrier Transport Engineering in Carbon

Nanotubes by Chirality-Induced Spin Polarization," ACS Nano **14**(3), 3389–3396 (2020).
[26] B.G. Cousins, A.K. Das, R. Sharma, Y. Li, J.P. McNamara, I.H. Hillier, I.A. Kinloch, and R.V. Ulijn, "Enzyme-Activated Surfactants for Dispersion of Carbon Nanotubes," Small **5**(5), 587–590 (2009).
[27] R. Contreras-Montoya, G. Escolano, S. Roy, M.T. Lopez-Lopez, J.M. Delgado-López, J.M. Cuerva, J.J. Díaz-Mochón, N. Ashkenasy, J.A. Gavira, and L. Álvarez de Cienfuegos, "Catalytic and Electron Conducting Carbon Nanotube–Reinforced Lysozyme Crystals," Adv. Funct. Mater. **29**(5), 1807351 (2019).
[28] S. Roy, and A. Banerjee, "Functionalized single walled carbon nanotube containing amino acid based hydrogel: a hybrid nanomaterial," RSC Adv. **2**(5), 2105–2111 (2012).
[29] D. Iglesias, M. Melle-Franco, M. Kurbasic, M. Melchionna, M. Abrami, M. Grassi, M. Prato, and S. Marchesan, "Oxidized Nanocarbons-Tripeptide Supramolecular Hydrogels: Shape Matters!," ACS Nano **12**(6), 5530–5538 (2018).
[30] Md.W. Rahman, M.C. Mañas-Torres, S. Firouzeh, J.M. Cuerva, L. Álvarez de Cienfuegos, and S. Pramanik, "Molecular Functionalization and Emergence of Long-Range Spin-Dependent Phenomena in Two-Dimensional Carbon Nanotube Networks," ACS Nano **15**(12), 20056–20066 (2021).
[31] Md.W. Rahman, M.C. Mañas-Torres, S. Firouzeh, S. Illescas-Lopez, J.M. Cuerva, M.T. Lopez-Lopez, L. Álvarez de Cienfuegos, and S. Pramanik, "Chirality-Induced Spin Selectivity in Heterochiral Short-Peptide–Carbon-Nanotube Hybrid Networks: Role of Supramolecular Chirality," ACS Nano **16**(10), 16941–16953 (2022).
[32] M. Anik Hossain, S. Illescas-Lopez, R. Nair, J. Manuel Cuerva, L. Álvarez de Cienfuegos, and S. Pramanik, "Transverse magnetoconductance in two-terminal chiral spin-selective devices," Nanoscale Horiz. **8**(3), 320–330 (2023).
[33] D. Zhang, K. Ryu, X. Liu, E. Polikarpov, J. Ly, M.E. Tompson, and C. Zhou, "Transparent, Conductive, and Flexible Carbon Nanotube Films and Their Application in Organic Light-Emitting Diodes," Nano Lett. **6**(9), 1880–1886 (2006).
[34] M.W. Rowell, M.A. Topinka, M.D. McGehee, H.-J. Prall, G. Dennler, N.S. Sariciftci, L. Hu, and G. Gruner, "Organic solar cells with carbon nanotube network electrodes," Appl. Phys. Lett. **88**(23), 233506 (2006).
[35] Y. Liu, J. Xiao, J. Koo, and B. Yan, "Chirality-driven topological electronic structure of DNA-like materials," Nat. Mater. **20**(5), 638–644 (2021).
[36] M. Atzori, C. Train, E.A. Hillard, N. Avarvari, and G.L.J.A. Rikken, "Magneto-chiral anisotropy: From fundamentals to perspectives," Chirality **33**(12), 844–857 (2021).
[37] J. Xiao, and B. Yan, "Magnetochiral Polarization and High Order Transport in DNA type Chiral Materials," ArXiv:2201.03623 (https://doi.org/10.48550/arXiv.2201.03623), (2023).
[38] T. Ando, "Spin-Orbit Interaction in Carbon Nanotubes," J. Phys. Soc. Jpn. **69**(6), 1757–1763 (2000).
[39] D. Huertas-Hernando, F. Guinea, and A. Brataas, "Spin-orbit coupling in curved graphene, fullerenes, nanotubes, and nanotube caps," Phys. Rev. B **74**(15), 155426 (2006).
[40] J.-S. Jeong, and H.-W. Lee, "Curvature-enhanced spin-orbit coupling in a carbon nanotube," Phys. Rev. B **80**(7), 075409 (2009).
[41] F. Kuemmeth, S. Ilani, D.C. Ralph, and P.L. McEuen, "Coupling of spin and orbital motion of electrons in carbon nanotubes," Nature **452**(7186), 448–452 (2008).
[42] G.A. Steele, F. Pei, E.A. Laird, J.M. Jol, H.B. Meerwaldt, and L.P. Kouwenhoven, "Large spin-orbit coupling in carbon nanotubes," Nat. Commun. **4**, 1573 (2013).
[43] Y. Piao, V.N. Tondare, C.S. Davis, J.M. Gorham, E.J. Petersen, J.W. Gilman, K. Scott, A.E. Vladár, and A.R. Hight Walker, "Comparative study of multiwall carbon nanotube nanocomposites by Raman, SEM, and XPS measurement techniques," Compos. Sci. Technol. **208**, 108753 (2021).
[44] M. Zdrojek, W. Gebicki, C. Jastrzebski, T. Melin, and A. Huczko, "Studies of Multiwall Carbon Nanotubes Using Raman Spectroscopy and Atomic Force Microscopy," Solid State Phenom. **99–100**, 265–268 (2004).
[45] G.T. Kim, E.S. Choi, D.C. Kim, D.S. Suh, Y.W. Park, K. Liu, G. Duesberg, and S. Roth, "Magnetoresistance of an entangled single-wall carbon-nanotube network," Phys. Rev. B **58**(24), 16064–16069 (1998).
[46] G. Baumgartner, M. Carrard, L. Zuppiroli, W. Bacsa, W.A. de Heer, and L. Forró, "Hall effect and magnetoresistance of carbon nanotube films," Phys. Rev. B **55**(11), 6704–6707 (1997).

[47] M. Jaiswal, W. Wang, K.A.S. Fernando, Y.-P. Sun, and R. Menon, “Magnetotransport in transparent single-wall carbon nanotube networks,” Phys. Rev. B **76**(11), 113401 (2007).
[48] K. Yanagi, H. Udoguchi, S. Sagitani, Y. Oshima, T. Takenobu, H. Kataura, T. Ishida, K. Matsuda, and Y. Maniwa, “Transport Mechanisms in Metallic and Semiconducting Single-Wall Carbon Nanotube Networks,” ACS Nano **4**(7), 4027–4032 (2010).
[49] V. Ksenevich, J. Galibert, V. Samuilov, V. Ksenevich, J. Galibert, and V. Samuilov, *Charge Transport in Carbon Nanotube Films and Fibers* (IntechOpen, 2010).
[50] A.B. Kaiser, G. Düsberg, and S. Roth, “Heterogeneous model for conduction in carbon nanotubes,” Phys. Rev. B **57**(3), 1418–1421 (1998).
[51] S.H. Lee, T.W. Uhm, Y.G. You, S.W. Kim, S.H. Jhang, U. Dettlaff-Weglikowska, and Y.W. Park, “Hall effect in carbon nanotube thin films,” Synth. Met. **198**, 84–87 (2014).
[52] S.N. Song, X.K. Wang, R.P.H. Chang, and J.B. Ketterson, “Electronic properties of graphite nanotubules from galvanomagnetic effects,” Phys. Rev. Lett. **72**(5), 697–700 (1994).
[53] L. Langer, L. Stockman, J.P. Heremans, V. Bayot, C.H. Olk, C. Van Haesendonck, Y. Bruynseraede, and J.-P. Issi, “Electrical resistance of a carbon nanotube bundle,” J. Mater. Res. **9**(4), 927–932 (1994).
[54] K.P. Maity, and V. Prasad, “Effect of chemical functionalization on charge transport of multiwall carbon nanotube,” Mater. Res. Express **6**(8), 0850a2 (2019).
[55] A. Bachtold, C. Strunk, J.-P. Salvetat, J.-M. Bonard, L. Forró, T. Nussbaumer, and C. Schönenberger, “Aharonov–Bohm oscillations in carbon nanotubes,” Nature **397**(6721), 673–675 (1999).
[56] C. Schönenberger, A. Bachtold, C. Strunk, J.-P. Salvetat, and L. Forró, “Interference and Interaction in multi-wall carbon nanotubes,” Appl. Phys. A **69**(3), 283–295 (1999).
[57] L.E. Hueso, J.M. Pruneda, V. Ferrari, G. Burnell, J.P. Valdés-Herrera, B.D. Simons, P.B. Littlewood, E. Artacho, A. Fert, and N.D. Mathur, “Transformation of spin information into large electrical signals using carbon nanotubes,” Nature **445**(7126), 410–413 (2007).
[58] Minghua Liu, Zhang, Li, and Wang, Tianyu, “Supramolecular Chirality in Self-Assembled Systems,” Chem. Rev. **115**(15), 7304–7397 (2015).
[59] G.-F. Liu, L.-Y. Zhu, W. Ji, C.-L. Feng, and Z.-X. Wei, “Inversion of the Supramolecular Chirality of Nanofibrous Structures through Co-Assembly with Achiral Molecules,” Angew. Chem. Int. Ed. **55**(7), 2411–2415 (2016).
[60] B. Yue, and L. Zhu, “Dynamic Modulation of Supramolecular Chirality Driven by Factors from Internal to External Levels,” Chem. – Asian J. **14**(13), 2172–2180 (2019).
[61] Y. Gong, Z. Cao, Z. Zhang, R. Liu, F. Zhang, J. Wei, and Z. Yang, “Chirality Inversion in Self-Assembled Nanocomposites Directed by Curvature-Mediated Interactions,” Angew. Chem. Int. Ed. **61**(10), e202117406 (2022).
[62] C. Gila-Vilchez, M.C. Mañas-Torres, J.A. González-Vera, F. Franco-Montalban, J.A. Tamayo, F. Conejero-Lara, J.M. Cuerva, M.T. Lopez-Lopez, A. Orte, and L. Álvarez de Cienfuegos, “Insights into the co-assemblies formed by different aromatic short-peptide amphiphiles,” Polym. Chem. **12**(47), 6832–6845 (2021).

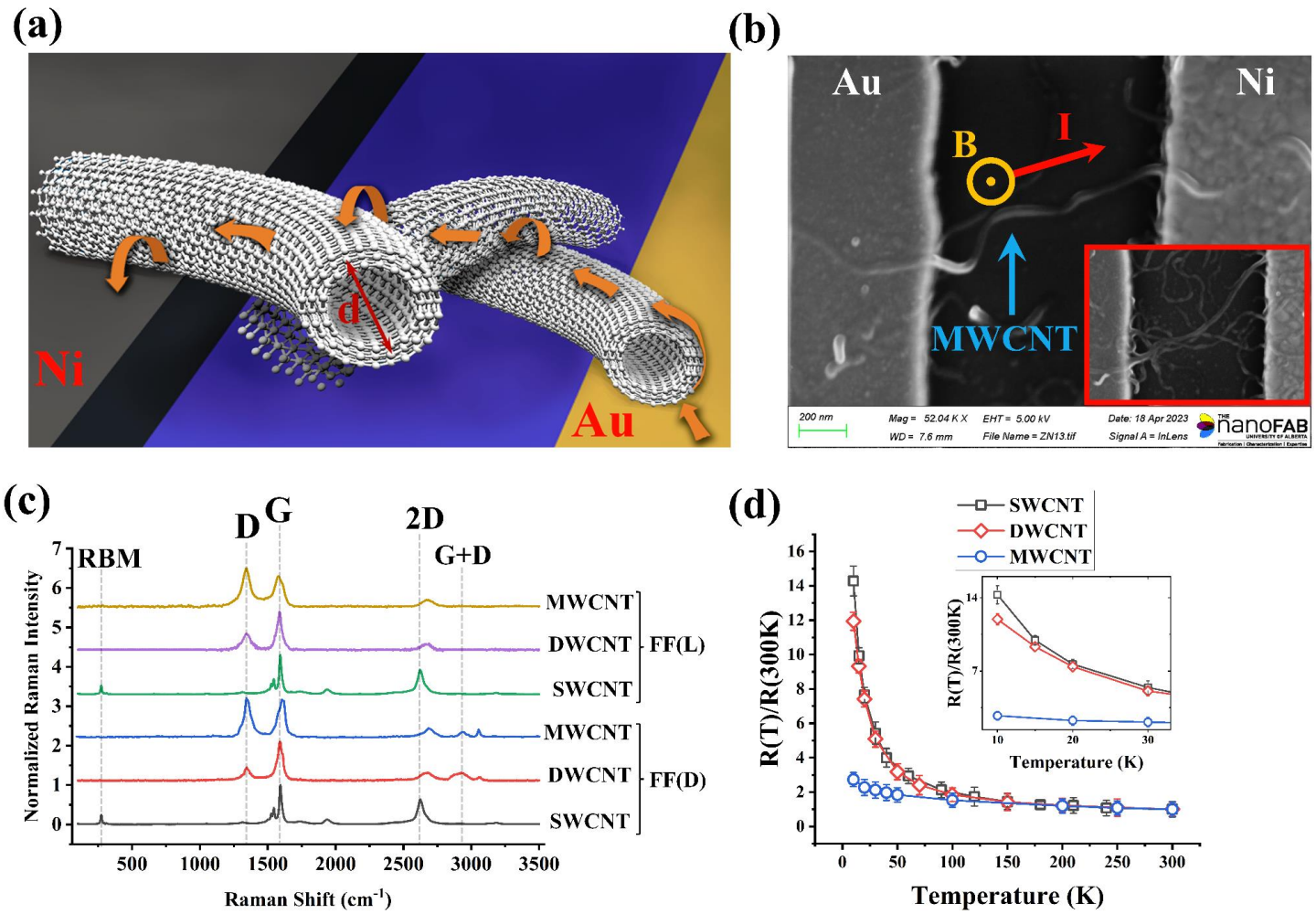

Figure 1. (a) Schematic diagram of CNTs connected between Au and Ni contacts. Electrical contacts are primarily with the outer shell of the tubes and the current path is primarily via the outer shell, as indicated by the arrows. (b) Scanning Electron Microscopic (SEM) image of the device. *Main image* shows a single MWCNT, contacted by an Au-Ni electrode pair. *Inset* shows a network of MWCNTs. Magnetic field *B* is perpendicular to the average direction of current (*I*) flow, which lies in the sample plane. (c) Raman characterization of the functionalized tubes, taken at 532 nm, showing the signature peaks. (d) Typical temperature-dependent resistance of the functionalized tubes.

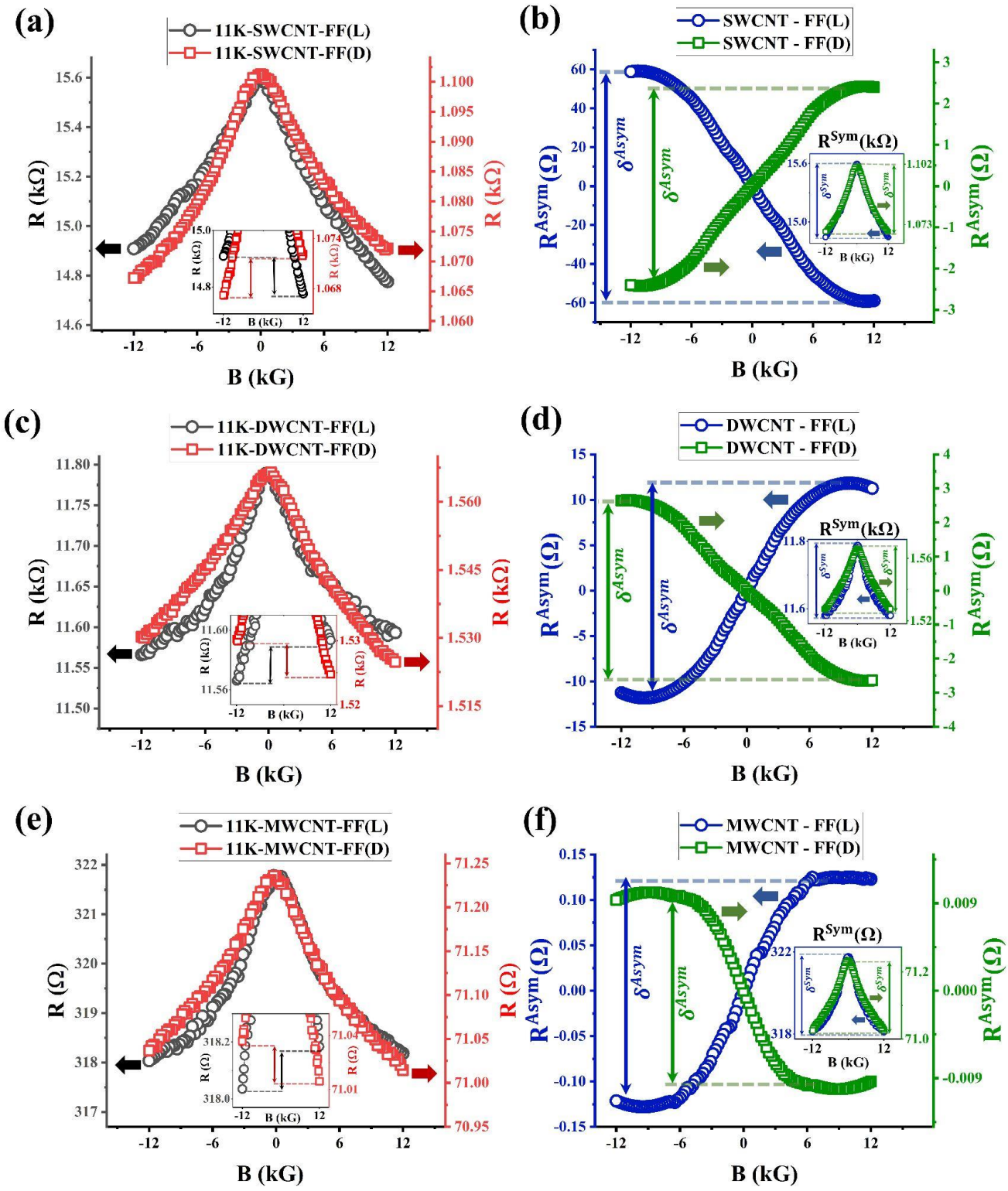

Figure 2. (a), (c), (e) Chirality-dependent MR effects in SWCNT, DWCNT and MWCNT networks respectively. (b), (d), (f) Asymmetric (*main image*) and symmetric (*inset*) components of the MR responses.

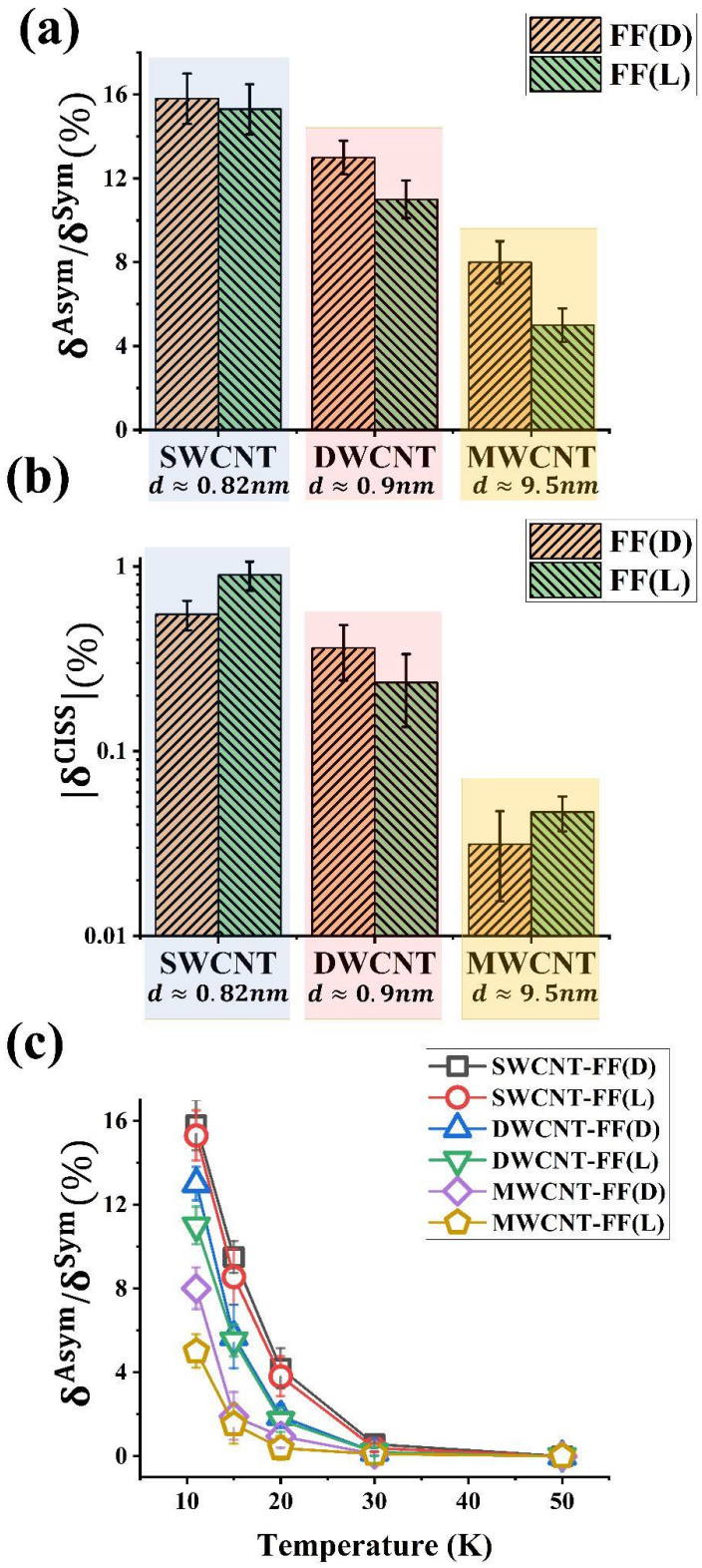

Figure 3. (a) CISS-induced asymmetry of the MR curves as a function of tube diameter. (b) CISS signal as a function of tube diameter. (c) MR asymmetry as a function of temperature for SW-, DW- and MWCNTs.

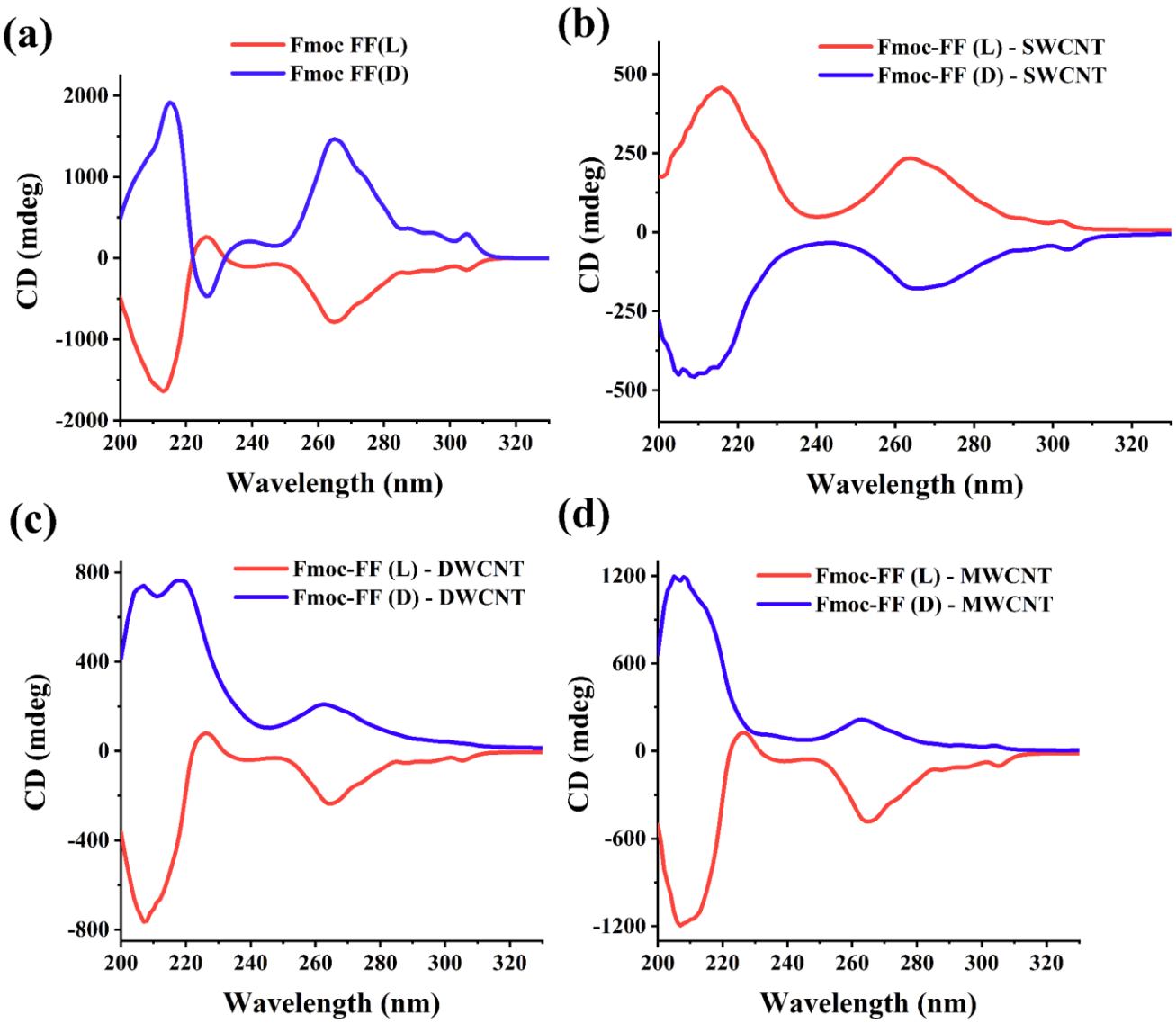

Figure 4. (a) CD spectra of the Fmoc-FF peptide solutions. (b) CD spectra of Fmoc-FF–SWCNT suspensions. (c) CD spectra of Fmoc-FF–DWCNT suspensions and (d) CD spectra of Fmoc-FF–MWCNT suspensions. In all measurements the peptide concentration was 5 mM and CNT concentration was 0.35%. Red color corresponds to the Fmoc-FF (L) derivative and blue color corresponds to the Fmoc-FF (D) derivative. CD spectra have been normalized for comparative purposes.